A Path-Planning Algorithm for Image-Guided Neurosurgery

Marc Vaillant[1], Christos Davatzikos[1]*, Russell H. Taylor[2], R. Nick Bryan[1]

[1] Neuroimaging Laboratory, Department of Radiology, Johns Hopkins University School of Medicine, 600 N. Wolfe street, Baltimore MD 21287
http://ditzel.rad.jhu.edu
[2] Department of Computer Science, Johns Hopkins University
3400 N. Charles street, Baltimore MD 21218

Abstract. A computer algorithm for determining optimal surgical paths in the brain is presented. The algorithm computes a cost function associated with each point on the outer brain boundary, which is treated as a candidate entry point. The cost function is determined partly based on a segmentation of the patients images into gray and white matter, and partly based on a spatially transformed atlas of the human brain registered to the patient's MR images. The importance of various structures, such as thalamic nuclei, optic nerve and radiations, and individual Brodman's areas, can be defined on the atlas and transferred onto the patient's images through the spatial transformation. The cost of a particular path associated with each critical structure, as well as the total cost of each path are computed and displayed, allowing the surgeon to define a low cost path, to visualize an arbitrary cross-section through the patient's MR images that contains this path, and to examine all the cross-sectional images orthogonal to that path.

1 Introduction

Modern tomographic imaging techniques have opened new and exciting opportunities for the surgical treatment of brain tumors, and for functional neurosurgery such as tremor treatment procedures. In particular, since magnetic resonance (MR) images show the internal structure of the human brain in great detail, a neurosurgeon can now use them to plan and perform procedures for the removal and biopsy of a tumor or its radiotherapeutic treatment, and for operating on delicate structures such as the globus pallidus and the thalamus, with substantially smaller risk than open craniotomies.

A key issue in image-guided neurosurgery is to effectively utilize the wealth of anatomical information provided by tomographic images in order to define an optimal surgical strategy. Such planning, however, is often a difficult task even for the experienced surgeon, for three reasons. First, because of the difficulty of mentally reconstructing the three-dimensional shape of brain structures from two-dimensional tomographic images. Second, because of the complexity of the

* Correspondences to Christos Davatzikos at the above address, e-mail: hristos@welchlink.welch.jhu.edu.

morphology of the human brain. Third, because the functional complexity of the human brain makes the prediction of the physiological consequences of various surgical plans a rather complicated task. Consequently, the surgeon can typically find a good path, but not necessarily the optimal path to approach a target.

Most stereotactic path planning systems [1, 2, 3, 4, 5, 6] rely on interactive visualization of proposed needle trajectories to avoid passage through critical structures. There has been some work to automate checking or generation of "safe" paths that completely avoid some critical structures. For example, Lavallee [6] extended this approach to provide automatic detection of potential intersections with blood vessels, based on stereo angiograms.

Because of its complexity, the problem of the surgical path planning can be effectively treated in a mathematical optimization framework. Several such frameworks have been investigated for automatically generating motion arcs for radiation beam therapy machines that intersect a tumor while minimally intersecting any designated "critical" structures [7, 8], although they typically rely on linear cost functions and constraints. In the system proposed here, we develop computationally efficient methods for scoring proposed paths based on nonlinear costs associated with destruction of *some* but not all of designated structures, for generating a complete map of such costs to assist selection of optimal trajectories, and for making allowances for uncertainties in tissue segmentation and intraoperative registration errors. Moreover, we utilize an anatomical brain atlas, adapted to the individual morphology of the patient's brain, to define regions of interest on the patient's images, such as cortical cytoarchitectonic sections and subcortical structures. Considering the complexity of the brain structure, the availability of automated ways of defining critical structures is very important for the effective use of path planning systems in the clinical practice.

In this paper we have focused on the relatively simpler problem of finding a single path from the outer boundary of the brain (the entry point of the surgical probe) to a target outlined in an MR image of the patient; this problem arises typically in the surgical biopsy of tumors and in tremor treatment procedures. Our methods however, can be extended to the relatively more complicated problem of finding optimal sets of beam paths in radiotherapy planning.

2 Methods

2.1 Path Planning Algorithm

In our approach we have incorporated information extracted from magnetic resonance images of the patient, and from a widely used anatomical atlas of the human brain [9], into a precise mathematical framework which quantifies the risk of damaging healthy brain tissue that is associated with a particular surgical strategy. Since the coordinates of the target point are predefined, the unknown parameters in this optimization problem are the coordinates of the entry point, denoted by $\mathbf{x}_e = (x_e, y_e, z_e)$. Our goal is to find the path that avoids, as much as possible, a number, S, of critical regions.

For each point in the three-dimensional image of the patient, and for each important structure (indexed by s), we first determine a function $m_s(\cdot)$, which reflects the cost for a surgical path passing through this particular point; this

function will be explained in detail later in this section. A second function, $f_s(\cdot)$, quantifies the penalty imposed to a particular path for damaging a fraction of a structure. This is typically a sigmoid function, whose value is small if only a small fraction of a structure is destroyed[3], but rises sharply above a threshold. This threshold can be different for different structures; regions of highly focal character (e.g. the primary motor or visual cortex) have a low threshold, while regions in which the function is more diffused have a higher threshold.

Our optimization problem is stated as follows: Find the path from a point $\mathbf{x}_e$ on the outer brain boundary to the target point $\mathbf{x}_t$, which minimizes the following cost function:

$$\mathcal{C}(\mathbf{x}_e) = \sum_{s=1}^{S} f_s \left(\int_0^1 m_s(\mathbf{x}(l)) dl \right) , \tag{1}$$

where $\mathbf{x}(l) = \mathbf{x}_e + (\mathbf{x}_t - \mathbf{x}_e)l, l \in [0,1]$, is a parameterization of the linear path connecting the entry point $\mathbf{x}_e$ with the target point $\mathbf{x}_t$.

The value of the function $m_s(\cdot)$, associated with the structure indexed by s, at a point reflects the importance of the tissue located at this particular point. In principle, in order to define $m_s(\cdot)$, the surgeon could outline structures of interest on each patient's images individually and assign a risk level to each outlined structure. Such approach, however, would be very laborious. Moreover, it would be limited by the fact that the MR images do not show all the details of the brain structure. For example, the divisions of the cortex into different cytoarchitectonic regions [10], each playing a different functional role, and the location of certain structures such as the optic nerve and radiations, and the individual thalamic nuclei, are not visible in the MR images.

Such structures are outlined in detail in anatomical atlases of the brain [11, 9], which can be therefore used for defining structures of interest. In order for anatomical atlases to be utilized in our path planning problem, however, they must be adapted to the individual morphology of the patient's brain. In our system we do this using an elastic transformation described in more detail in the appendix. The surgeon can define the value of the function $m_s(\cdot)$ in each structure in the atlas, depending on its importance. The assigned values are then mapped onto the patient's brain through the registration transformation.

In addition to structures defined through the spatially transformed atlas, structures defined directly on the MR images of the patient are also used to determine the function $m_s(\cdot)$. In particular, we have used a fuzzy c-means segmentation method [12, 13] to determine the cortical region; $m_s(\cdot)$ is then set to a higher value on the segmented cortex and a lower value elsewhere.

In principle, having defined the structures of interest in the MR image and the associated risk levels, we could find the path that minimizes the cumulative cost in (1). In practice, however, one must account for errors in mapping the image coordinates to the physical coordinates in the patient's brain, i.e. in errors

[3] This reflects the ability of the brain to compensate for the loss of neurons by utilizing alternative ways of processing information.

of the localizing devices, as well as for errors in the registration between atlas and MR images. We do this by applying a spatial filtering to each structure of interest; this effectively widens the spatial extent of each structure, typically by a few millimeters, accounting for the localization and registration errors. The type and size of the filtering kernel can be controlled by the surgeon. In our experiments we have used a Gaussian filter. It is important to note that (1) holds if this filtering procedure causes structures to overlap, because $m_s(\cdot)$ along each path is integrated separately for each structure. This allows $f_s(\cdot)$ to be different for each structure.

2.2 Software Description

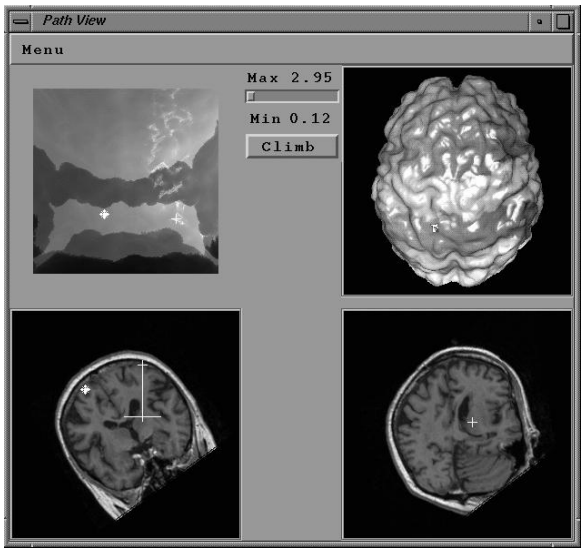

Fig. 1. The layout of the path planning software interface. The upper right window shows a 3D rendering of the outer boundary of the brain with cost superimposed in a color scale. The planar domain in which this surface is parameterized is displayed in the upper left window. The lower left window displays a cross-section through the MRI volume containing a particular trajectory. The lower right window displays cross-sectional images oriented perpendicularly to the surgical path. The surgeon can visualize the cost associated with each entry point on the outer boundary of the brain, can click on a particular entry point on the upper left window (which is also displayed on the 3D rendered surface on the upper right window) and visualize any cross-section containing the corresponding path in lower left window, as well as visualize the orthogonal cross-sections of that path in the lower right window.

A layout of the software interface is shown in Fig. 1. The upper right window shows a 3D rendering of the outer boundary of the brain, using the OpenGL graphics library. This surface is determined in two steps: in the first step, the brain tissue is extracted from a volumetric magnetic resonance image of the

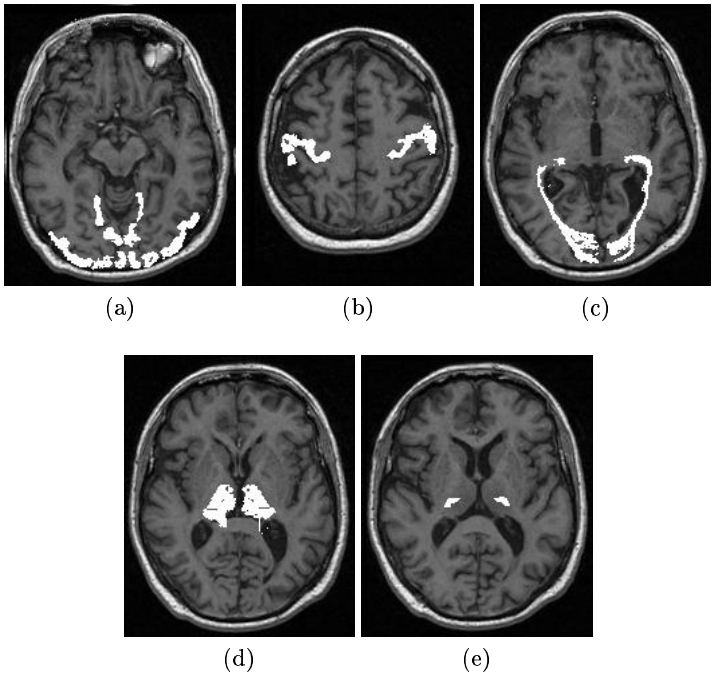

Fig. 2. Overlay of selected critical structures on the MRI images. The structures were determined by spatially transforming the Talairach atlas into registration with the MR image. (a) Brodman areas 17-19 (b) Brodman areas 1-4, (c) Optic radiations, (d) Thalamus, (e) VPL nucleus (the target).

patient, and in the second step, a parameterization of the outer brain boundary is found using a deformable surface algorithm.

In order to extract the brain tissue in the first step, we use a thresholding followed by a morphological erosion [14] which isolates the brain tissue from the surrounding tissues (dura, skin, fat, etc.). A 3D seeded region growing is then used to extract the brain tissue. Finally, a morphological conditional dilation is applied to recapture the tissue that was lost in the erosion step.

In the second step, a deformable surface algorithm [15, 16] is applied to the skull-stripped images. The surface is initialized in a spherical configuration surrounding the brain, and deforms elastically under an image-derived force field, wrapping around the outer surface of the brain. This surface is defined on a planar parametric domain, which is displayed in the upper left window in Fig. 1.

The user can select a number of structures of interest from a list, and calculate the cost of the path connecting each point on the outer cortical surface, which is typically sampled with 80,000 polygons, to a prespecified target point. The cost is displayed in a color scale on the rendered surface, and in gray scale on the parametric domain. The gray-scale representation of the color is that darker

regions in the upper right window of Fig. 1 (actually displayed as blue in color) correspond to relatively safer areas. The actual gray scale representation of cost, in the upper left window of Fig. 1, is that bright regions correspond to safer areas. The user can then visualize a particular path by defining the entry point on the parametric domain (the point is simultaneously displayed on the rendered surface), and a second point needed to uniquely define a cutting plane together with the entry and target points. The resulting cross-sectional image containing the path is displayed in the bottom left window (see Fig. 1) and the user can scroll through cross-sectional images, displayed in the bottom right window, oriented perpendicularly to a selected path. Finally, the graphical user interface allows the user to interactively change the subset of structures and the function $f_s(\cdot)$ for each structure; recalculation of the cost for each possible entry point is then very fast because $\int_0^1 m_s(\mathbf{x}(l))dl$ has already been computed resulting in nearly immediate update of the display.

3 Experiments

In the experiment presented in this section, we chose the VPL thalamic nucleus as our targeted region in a subject. The critical structures were the cortex that was determined from the MR images of the subject, and the optic radiations, the thalamus, and Brodman areas 1-3, 4, 17-19, 22, 41-42, representing somatosensory cortex, motor cortex, visual cortex, and auditory cortex, which were determined from the spatially transformed Talairach atlas. The registered VPL nucleus was superimposed on the 3D data set(see Fig. 2e), and a target within this region was manually selected. The outer surface of the brain was extracted using the procedure described in Sect. 2.2. The function $m_s(\cdot)$ for each structure and the type and size of the smoothing filter were then set to unity on the critical structures and zero elsewhere. The cost $\mathcal{C}(\mathbf{x}_e)$ was then computed for each entry point $\mathbf{x}_e$ on the outer brain boundary. Run time for the atlas registration procedure was approximately 3 minutes and the cost calculation for these structures was approximately 30 seconds on an SGI Onyx running with R10000 processors.

The resulting cost associated with each possible entry point is mapped to the planar domain in which the brain boundary is parameterized (see Fig. 3a, and Fig. 4), and to a color scale on the rendered surface (see Fig. 3b). The brighter regions in Fig. 3a and Fig. 4 indicate relatively safer areas of entry which in this experiment are localized along the gyri of the left hemisphere (images are displayed in radiology convention) away from the posterior and central regions of the brain. These results are in agreement with the entry location which would be typically chosen by a neurosurgeon. The target was in the thalamus of the left hemisphere (**right** side of the images, according to the radiology convention), so one would expect safer entry on the left side of the brain in order to minimize the total amount of brain tissue at risk (Fig. 4d). Entry along the gyri is safer because the cortex is oriented orthogonal to the path's direction, therefore the amount of cortical tissue near the path's trajectory would be minimized(Fig. 4a). The posterior and central regions of the outer surface are high risk for entry because a substantial amount of the functionally important regions, defined by

the Brodman areas and optic radiations, would be destroyed along the path's trajectory (Fig. 4b and 4c).

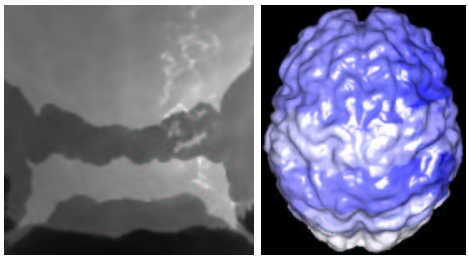

(a) (b)

Fig. 3. Total risk associated with each possible entry point on the outer boundary of the brain. (a) The total risk is superimposed on the planar domain in which the boundary was parameterized, with brighter regions being the relatively safer entry points. (b) The total risk superimposed on the 3D rendered surface. Here, the darker a region is (the brighter blue, in color), the safer the entry point is. There is a one to one correspondence between the points in (a) and those in (b).

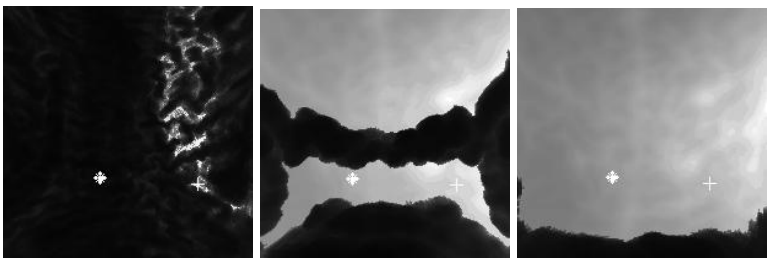

(a) (b) (c)

Fig. 4. Planar domain of the (flattened) outer cortical surface with cost displayed in gray scale. Bright regions indicate safe points of entry. (a) Cortex, (b) Brodman areas, and (c) Optic radiations. The dark regions in (b) reflect the risk of damaging the primary motor, auditory, and visual cortex. The dark region in (c) reflects the risk of damaging the optic radiations.

4 Summary and Conclusion

We have presented a computer algorithm for path planning in neurosurgical procedures. The algorithm utilizes information extracted from magnetic resonance images of the patient's and from an anatomical atlas adapted to the brain morphology of the patient, and it computes a risk associated with each possible entry point along the outer boundary of the brain. The risk associated with a

particular structure defined either on the atlas or on the patient's images can be separately computed and visualized. A graphical user interface allows the surgeon to visualize cross-sectional images either containing a particular path or being orthogonal to it.

Several extensions of this work are possible. For example, functional and angiographic images of the patient can be readily incorporated into the cost calculation procedure. Moreover, the system can be linked to lesion/deficit databases [17], which can provide valuable cues to the surgeon of the physiological effects that are likely to result from lesioning a particular region in the brain. Finally, empirical knowledge of the surgeon can also be incorporated into the system as an additional risk function defined either on the entire brain or on selected structures.

In this paper we have addressed the relatively simpler problem of finding a single surgical path. Our current direction in this work is the extension of our algorithm to the relatively more complex problem of finding a configuration of multiple paths. The latter problem is a key issue in image-guided radiotherapy in which an optimal radiation beam configuration is sought, which delivers maximal radiation to the target while minimizing the radiation delivered to the surrounding healthy tissue.

5 Acknowledgments

The authors would like to thank Tim Eckel for suggesting the Brodman areas used in the experiment and Tushar Goradia for his suggestions in the initial planning of this work. This work was partially supported by a grant from the American Cancer Society.

6 Appendix

In order to obtain a shape transformation that adapts the Talairach atlas to the individual brain morphology of a patient, we use an elastic transformation method (see [18, 19] for more details). The basis of this method is a map that corresponds regions along the outer cortical surface in the atlas and homologous regions in the MR image. In order to find such a map, a parameterization of the outer cortical surface is first obtained for both the atlas and the MR image, using a deformable surface algorithm [16, 15]. Specifically, a deformable surface is initialized at a spherical configuration surrounding the cortex, and is let free to deform, adapting to the shape of the brain. Since this surface is defined in a planar parametric domain, denoted by $\mathcal{D}$, a parametric representation of the outer cortex is readily obtained after convergence of the algorithm.

Using this parametric representation, various curvatures can then be calculated using the principles of differential geometry [20]. In our algorithm we find the minimum, the maximum, and the Gaussian curvatures, which reflect different but complementary aspects of the cortical structure [15]. We then find a reparameterization of the outer cortex of the atlas that brings its curvature maps into best agreement with those derived from the MR image. This is accomplished by finding an elastic deformation of the parametric domain $\mathcal{D}$ onto itself, which is driven by external force fields that attempt to align the curvature

maps of the atlas and the MR image. This reparameterization does not alter the shape of these surfaces, i.e. it does not alter their extrinsic geometry; it simply applies a local stretching or shrinking according to the local curvatures.

After the map from the outer cortex in the atlas to that in the MR image has been determined, it is used to derive a three-dimensional elastic transformation of the atlas, bringing it into register with the MR image. In order to account for major structural abnormalities, such as the often dramatic ventricular expansion found in elderly individuals and tumor growth that pushes the surrounding tissue, we use the framework of pre-strained elasticity (in this paper we deal only with the ventricular expansion). In this framework, the atlas is not assumed to be in equilibrium in its reference (undeformed) configuration. Instead, it has a non-zero strain energy distributed uniformly throughout the ventricles. As this strained configuration is relaxed, it results in the expansion of the ventricles. The value of the stress that drives this expansion is determined from the ratio of the ventricular volumes in the atlas and the MR image.

The ventricular expansion described above is only a gross shape correction, and it results in a rough alignment in the ventricular and peri-ventricular regions. Since the latter region is often very important, especially in tremor treatment procedures, a finer alignment of the ventricular boundaries is obtained using a force field derived from the image data. This field causes the mutual attraction of the ventricular boundaries in the warped atlas and in the MR image, as shown schematically in Fig. 5, resulting in their alignment.

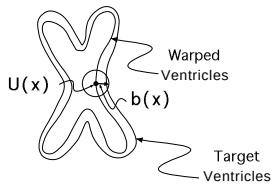

Fig. 5. The forces that align the ventricular boundaries. The surrounding structures are rearranged by the elastic forces.

References

1. A.C.F. Colchester, J. Zhao, K.S. Holton-Tainter, et.al. Development and preliminary evaluation of VISLAN, a surgical planning and guidance system using intra-operative video imaging. *Medical Image Analysis*, 1:73–90, 1996.
2. T. Peters, B. Davey, P. Munger, R. Comeau, A. Evans, and A. Olivier. Three-dimensional multimodal image guidance for neurosurgery. *IEEE Trans. on Med. Imaging*, 15:121–128, 1996.
3. W.E.L. Grimson, G.J. Ettinger, S.J. White, T. Lozano-Perez, W.M. Wells III, and R. Kikinis. An automatic registration method for frameless stereotaxy, image

guided surgery, and enhanced reality visualization. *IEEE Trans. on Med. Imaging*, 15:129–140, 1996.
4. B.A. Kall. Comprehensive multimodality surgical planning and interactive neurosurgery. *Computers in Stereotactic Neurosurgery*, pages 209–229, 1992.
5. H.H. Ehricke, G. Daiber, R. Sontag, W. Strasser, M. Lochner, L.R. Schad, and W.J. Lorenz. Interactive 3-D graphics workstations in stereotaxy: Clinical requirements, algorithms and solutions. *Proc. of Vis. in Biomed. Comp. Conf.*, SPIE 1808:548–558, 1992.
6. R.H. Taylor, S. Lavalle, G.C. Burdea, and R. Mosges, Editors. *Computer-Integrated Surgery*. MIT Press, 1995.
7. S. Webb. Optimization by simulated annealing of three-dimensional conformal treatment planning for radiation fields defined by a multileaf collimator. *Phys. Med. Biol.*, 36:1201–1226, 1991.
8. R. Tombropoulos, A. Schweikard, J.C. Latombe, and J.R. Adler. Treatment planning fro image-guided robotic radiosurgery. *Proc. of the Conf. on Comp. Virt. Real. in Med., CVRMED'95*, pages 131–137, 1995.
9. J. Talairach and P. Tournoux. *Co-planar Stereotaxic Atlas of the Human Brain*. Thieme, Stuttgart, 1988.
10. K. Brodman. *Vergleichende Lokalisationslehre der Grosshirnrinde*. Barth, Leipzig, 1908.
11. G. Schaltenbrand and W. Wahren. *Atlas of Stereotaxy of the Human Brain*. Tieme Verlag, Stuttgart, 1977.
12. L.O. Hall, A.M. Bensaid, et.al. A comparison of neural network and fuzzy clustering techniques in segmenting magnetic resonance images of the brain. *IEEE Trans. on Neural Networks*, 3:672–682, 1992.
13. D. Pham, J.L. Prince, A.P. Dagher, and C. Xu. An automated technique for statistical characterization of brain tissues in magnetic resonance imaging. *Submitted*, 1996.
14. E. Dougherty and C. Giardina. *Image Processing – Continuous to Discrete*, volume 1. Prentice-Hall, 1987.
15. C. Davatzikos and R.N. Bryan. Using a deformable surface model to obtain a shape representation of the cortex. *IEEE Trans. on Med. Imaging*, 15, Dec. 1996.
16. C. Davatzikos and R.N. Bryan. Using a deformable surface model to obtain a mathematical representation of the cortex. *Proc. of the IEEE Comp. Vision Symp.*, pages 212–217, Nov. 1995.
17. S.H.J. Whitehead, R.N. Bryan, S. Letovsky, C. Paik, J. Miller, and J. Gerber. A database for brain structure/function analysis. *Proc. of the Am. Soc. of Neuroradiology Conf.*, page 166, 1994.
18. C. Davatzikos. Spatial normalization of 3D images using deformable models. *J. Comp. Assist. Tomogr.*, 20:656–665, July/August 1996.
19. C. Davatzikos. Nonlinear registration of brain images using deformable models. *Proc. of the Workshop on Math. Meth. in Biom. Image Anal.*, pages 94–104, June 1996.
20. R. Millman and G. Parker. *Elements of Differential Geometry*. Prentice Hall, 1977.